















Cite this: *RSC Adv.*, 2024, **14**, 22504

Dansyl fluorophore functionalized hierarchically structured mesoporous silica nanoparticles as novel latent fingerprint development agents†

Lais F. A. M. Oliveira, ^a Lais V. A. T. da Silva, ^a Artur F. Sonsin, ^a Meclycia S. Alves, ^a Cristiane V. Costa, ^a Jeane C. S. Melo, ^a Nicholas Ross, ^b Paul T. Wady, ^c Thomas Zinn,^c Ticiano G. do Nascimento, ^a Eduardo J. S. Fonseca, ^a Alexandro M. L. de Assis, ^{ade} A. Robert Hillman ^{*b} and Adriana S. Ribeiro ^{*a}

A nanostructured hybrid material based on mesoporous silica nanoparticles (MCM-41) functionalized with chitosan and a fluorescent dye (dansylglycine), designated MCM-41@Ch@DnsGly, was synthesized and characterized with a view to its application for the visualization of latent fingerprints. These nanoparticles were applied as latent fingerprint developers for marks on surfaces of diverse chemical composition, topography, optical characteristics, and spatially variant nature, typical of forensically challenging evidence. For quality assessment of the enhanced fingermarks, the developed images were analyzed holistically using the UK Home Office scale, forensic protocols and, in terms of their constituent features (minutiae), using forensic software. Across a substantive collection of marks deposited on chemically diverse surfaces and subject to complex environmental and temporal histories, 94% of the enhanced images presented sufficient minutiae for comparison with model dactyloscopy images. This novel nanomaterial presents enhanced performance with significant promise for superior exploitation by forensic practitioners in the acquisition and analysis of crime scene evidence.

Received 25th April 2024
Accepted 4th July 2024
DOI: 10.1039/d4ra03074e
rsc.li/rsc-advances

Introduction

The papillary ridge patterns present on the tips of human fingers, which remain topologically unchanged during (and beyond) the life of an individual, provide the primary method of personal identification in criminal investigations. Thus, from the moment that the surface of an object is touched by a finger, sweat and oily substances can be transferred and deposited onto the surface, resulting in the formation of a fingerprint.^{1–3} Nevertheless, fingerprints (strictly, fingermarks) that are recovered at crime scenes are frequently non-visible (latent) and thus require the use of physicochemical development techniques to enhance their visibility to the naked eye and make them interpretable for forensic purposes.⁴ Conventional fingerprint

development approaches include optical, physical, and chemical processes, involving chemical reaction or interaction between the developing agent (commonly a colored or fluorescent reagent) and component(s) of the fingerprint residue. A wide range of chemical agents, based on simple powders (metal or metal oxide), cyanoacrylate fuming, silver nitrate, ninhydrin, and small particle reagent (SPR) is commercially available. These offer simplicity of application, ease of operation and efficiency,^{3,5,6} but with limits to the circumstances in which they can recover latent fingerprints of adequate quality for forensic identification.

Recently, innovative methodologies based on mass spectrometry,⁷ spectroscopy,⁸ electrochemistry,^{9–17} and nanoparticles^{18–20} have enhanced the performance of latent fingerprint development.²¹ These reagents and technologies hold the promise of efficient development of latent fingerprints with improved contrast, sensitivity, and selectivity, as well as low reagent toxicity.^{11,22} Amongst these, the facility to tune nanomaterial characteristics motivates further improvements in sensitivity and selectivity for visualizing both fresh and aged latent fingerprints.^{20–28}

Mesoporous silica nanoparticles (MSNs) have attracted special attention following discovery of a new family of molecular sieves designated M41S; this includes MCM-41, MCM-48 and SBA-15. They are highly attractive as drug carriers, and

^aFederal University of Alagoas, Campus A. C. Simões, 57072-970, Maceió, AL, Brazil. E-mail: aribeiro@qui.ufal.br

^bDepartment of Chemistry, University of Leicester, Leicester LE1 7RH, UK. E-mail: arh7@leicester.ac.uk

^cDiamond Light Source, Harwell Science and Innovation Campus, Didcot OX11 0DE, UK

[†]Technical and Scientific Section of Alagoas, Federal Police, 57025-080, Maceió, AL, Brazil

^{*}National Institute of Criminalistics, Federal Police, 70610-902, Brasília-DF, Brazil

† Electronic supplementary information (ESI) available: XRD and SAXS results, images of developed fingerprints. See DOI: <https://doi.org/10.1039/d4ra03074e>



for diagnostics, catalysis, separation and sensing,^{29–31} as a consequence of their unique combination of attributes. These include controlled particle size, porosity (pore size ranging from 2–10 nm), morphology (2D-hexagonal and 3D-cubic structures), high specific surface area, high chemical stability, and ease of surface functionalization. Here we exploit these desirable characteristics – notably high surface area and surface modification – for the case of MCM-41 to enhance the interaction between the development reagent and fingerprint residue.

Notwithstanding the above attractive attributes, MSNs still have shortcomings, since it is difficult to achieve monodisperse particles of controllable size. This is because the surface of the MSNs contains a large number of hydroxyl groups and presents a high energy surface, making them prone to agglomeration and difficult to re-disperse. Modification of the nanoparticles is a convenient way to reduce their surface energy and facilitate their dispersion.³² Polymers are the preferred materials for this purpose, since they offer structural diversity and a range of chemical functionalities. Consequently, significant effort has been invested in fabricating versatile MSN surfaces by coating them with polymers such as alginate, chitosan, polyethylene glycol (PEG), and Pluronic P123.^{30,31,33}

The strategy we pursue here employs chitosan as the MCM-41 derivatizing agent. This choice is based on successful application of chitosan modified nanoparticles in drug delivery systems and gene therapy (in the pharmaceutical area),^{32,34,35} and for stabilization of food-grade emulsions.³⁶ More recently, forensic application of chitosan modified microparticles has exploited their polycationic nature and ability to bind to fingerprint lipid residues by both electrostatic and lipophilic interactions.^{37,38} Hejjaji *et al.*³⁷ have prepared chitosan microparticles modified with tripolyphosphate for visualization of latent fingerprints and Vučković *et al.*³⁸ improved the fingerprint development process by adding L-lysine to the system. However, there are few studies employing chitosan for detection and enhancement of latent fingerprints and, to the best of our knowledge, no reports of the use of hierarchically structured MSNs modified with chitosan (MSN@Ch) for such applications – the strategy here.

We have synthesized and characterized a series of modified chitosan derivatives based on red propolis,³⁹ silver nanoparticles,⁴⁰ polyaniline/clay composites^{41,42} and dansyl fluorophores^{43,44} as materials for exploitation in pharmaceutical, biological, electrochromic device and fluorescence sensing applications. Amongst these, dansyl derivatives aroused considerable interest as materials for latent fingerprint development,^{45,46} since they exhibit intense absorption bands in the near UV region and strong fluorescence in the visible region with high emission quantum yields; the synthetic versatility of the sulfonyl group is an additional attraction.⁴⁷ Our materials fabrication strategy also recognizes the common requirement of fluorescent small organic molecules (typified by dansyl derivatives) to be incorporated into another matrix to address their low biocompatibility, low water solubility, and toxicity.^{5,20,48}

In previous work on the visualization of latent fingerprints,⁴⁵ we have made use of the dansylglycine fluorophore, delivered *via* the vehicle of electrospun fluorescent polycaprolactone

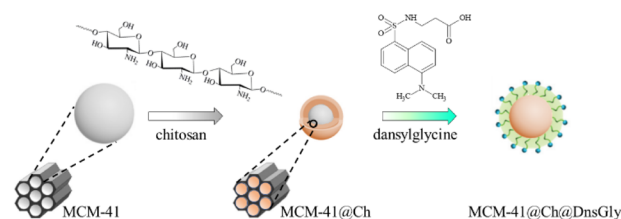
(PCL)/dansylglycine nanofibers. The present work delivering the same fluorophore, but *via* MCM-41@chitosan@dansylglycine nanoparticles, offers two significant practical advantages. First, the nanofiber approach requires a laboratory infrastructure (including a fume hood for safety reasons, and a high potential source (~20–30 kV)), while the nanoparticles require no such facilities and can thus be applied at a crime scene. Second, the effectiveness of the nanofiber material was found to be restricted to latent fingerprints on metallic surfaces (typified by knife blades and bullet cartridge cases) while the MCM-41-based nanoparticles are effective on a wider range of surfaces, illustrated here by glass, plastic, cartridge cases, and polymer banknotes.

The overarching aim of the present study is a versatile and effective latent fingerprint visualization material based on MSNs, chitosan and dansyl derivatives. The strategy for accomplishing this (shown in Scheme 1) builds on and extends previous knowledge on the synthesis of chitosan-based dansyl materials.^{43,44} Specific objectives en route to this are (i) structural characterization of MCM-41@Ch@DnsGly (DnsGly = dansylglycine) nanoparticles; (ii) fluorescence characteristics of the dansyl-functionalized NPs; (iii) exploitation of the NP fluorescence characteristics in the visualization of latent fingerprints on metal, polymer (simplistically, “plastic”) and glass substrates; and (iv) a means of evaluating the quality of developed images based on a forensic protocol for fingerprint examinations including observation at whole mark (first level, pattern type) and individual features (second level, minutiae, detail).

Results and discussion

Structural characterization

The FTIR spectrum of MCM-41 (see Fig. 1) shows a band at 3446 cm^{−1} ascribed to the hydroxyl functionality within adsorbed water molecules and surface silanols (Si–OH).⁴⁹ There are also absorption peaks arising from asymmetric (1244 cm^{−1}, 1068 cm^{−1}) and symmetric (968 cm^{−1}) Si–O–Si vibrations. The band at 1630 cm^{−1} is attributed to the vibration of adsorbed H₂O^{29,50,51} and the band at 803 cm^{−1} corresponds to the asymmetric vibration of Si–OH associated with the formation of the condensed silica structure.^{29,52,53} In the MCM-41@Ch spectrum, the absorption bands at *ca.* 3130 cm^{−1} and 1549 cm^{−1} are characteristic of stretching and bending vibrations of the –NH₂



Scheme 1 Modification of the MCM-41 NPs with chitosan, followed by surface modification of MCM-41@Ch with DnsGly through interaction between the hydroxyl groups of chitosan and carboxylic acid groups of dansylglycine (see Scheme S1, ESI†).



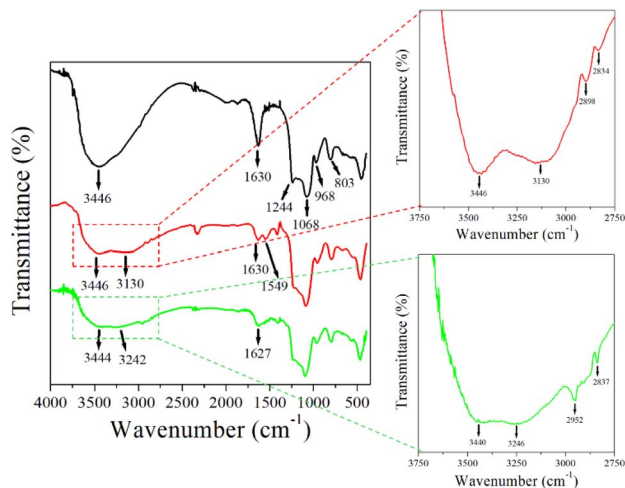


Fig. 1 FTIR spectra for MCM-41 (—), MCM-41@Ch (—) and MCM-41@Ch@DnsGly (—). See main text for commentary on marked features.

group^{42,44,50} related to chitosan (and/or APTES). The absorption band at 1630 cm^{-1} is attributed to the stretching mode of the $\text{C}=\text{O}$ carbonyl group within the *N*-acetyl units (the degree of deacetylation of chitosan is $\sim 85\%$ ⁴⁴). The bands around 2870 cm^{-1} corresponding to the $\text{C}-\text{H}$ stretching mode in chitosan, and the absorption bands at 1151 cm^{-1} (anti-symmetric stretching of $\text{C}-\text{O}-\text{C}$ bridge) and 1070 cm^{-1} (skeletal vibration involving the $\text{C}-\text{O}$ stretching) characteristic of its saccharide structure are overlapped by bands associated with MCM-41 that are also present in this region.

The MCM-41@Ch@DnsGly absorption spectra present a similar feature to that observed in the MCM-41@Ch spectrum. The absorption bands attributed to the $-\text{OH}$ and $-\text{NH}_2$ stretching vibrations are broader, suggesting the formation of hydrogen bonds between the chitosan and dansylglycine moieties.⁵⁴ However, the bands related to the DnsGly are not clear due to the prevalence of MCM-41@Ch with respect to the amount of the DnsGly (5%) in the sample.

XRD data for MCM-41, MCM-41@Ch and MCM-41@Ch@DnsGly (see Fig. S1a, ESI†) are very similar in the region $2\theta > 10^\circ$. The broad feature seen in each case indicates that the dansylglycine-chitosan-modified and unmodified NPs are amorphous. For $2\theta < 10^\circ$, the responses for the modified MCM-41 nanoparticles are distinctly different to that for the unmodified material. For greater insight into this, we turn to SAXS data, in which MCM-41 exhibited one well-resolved peak and other two broad peaks, indexed as (100), (110) and (200) reflections, respectively, corresponding to an ordered 2D hexagonal system. The scattering intensities of MCM-41, MCM-41@Ch and MCM-41@Ch@DnsGly are reported as a function of the scattering vector Q (Fig. S1b, ESI†). The SAXS peaks of MCM-41 show an intense (100) peak at 0.19 \AA^{-1} , and two low intensity reflections at 0.29 \AA^{-1} and 0.36 \AA^{-1} that are characteristic of hexagonal structures, consistent with values reported in the literature.^{55,56} After modification with chitosan, the ordered structure of nanocomposites was changed, since the SAXS

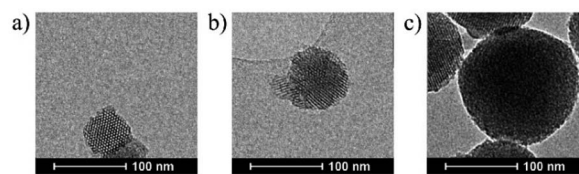


Fig. 2 Representative TEM images of (a) MCM-41, (b) MCM-41@Ch and (c) MCM-41@Ch@DnsGly.

analysis revealed a shift and an apparent decrease in intensity of the (100) diffraction peaks for MCM-41@chitosan and MCM-41@chitosan@DnsGly, besides the disappearance of the (110) and (200) reflection peaks. This structural disorder may be explained by the partial filling of the MCM-41 pores with the chitosan.

The morphologies and microstructures of the as-prepared and modified MCM-41 NPs were determined using TEM (see Fig. 2). The TEM image of the as-prepared MCM-41 (Fig. 2a) shows a highly ordered mesoporous network with a hexagonal array. After functionalization with chitosan, it is possible to observe in the MCM-41@Ch NPs TEM image (Fig. 2b) a slight modification in the ordered pattern of MCM-41, suggesting that chitosan may have partially filled the mesoporous channels of the MCM-41. Further, it is possible to observe in Fig. 2c that the dansylglycine entirely covers the MCM-41@Ch NPs.

The TEM images of unmodified MCM-41 and the surface modified nanoparticles (MCM-41@Ch and MCM-41@Ch@DnsGly) show spherical shapes, with average particle size (diameter) of 68, 82 and 113 nm, respectively (see Fig. 3).

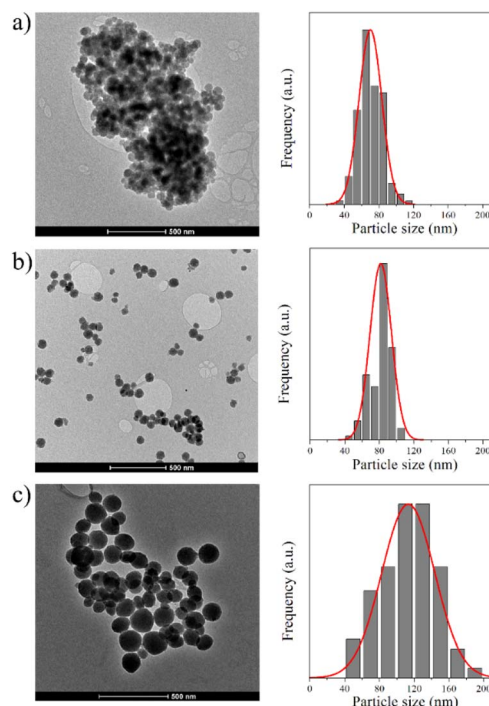


Fig. 3 TEM images of (a) MCM-41, (b) MCM-41@Ch and (c) MCM-41@Ch@DnsGly and their particle size distribution histograms.



The size of Ch and Ch@DnsGly modified MCM-41 NPs was larger than unmodified MCM-41 NPs and they did not vary considerably as shown by the size distribution histograms (Fig. 3). While bearing in mind the nature of the TEM sample preparation (deposition on a grid), we find no evidence for significant agglomeration of particles after surface modification.

Fluorescence properties of the NPs

The solid-state photoluminescence (PL) spectra of MCM-41, MCM-41@Ch, and MCM-41@Ch@DnsGly NPs and of DnsGly are shown in Fig. 4a. It is well known that dansyl derivatives are fluorescent, showing greenish to yellow light emission in the range of 500–550 nm for the fluorophores dissolved in organic solvents such as CH_2Cl_2 and CH_3CN .^{43,45} Anchoring DnsGly on the MCM-41@Ch surface causes a slight bathochromic shift in the emission wavelength of the MCM-41@Ch@DnsGly NPs ($\lambda_{\text{em}} = 515$ nm) and broadening of the emission band, as compared to pristine DnsGly ($\lambda_{\text{em}} = 500$ nm). This is attributed to hydrogen bonding between the carbonyl group of chitosan and the carboxylic acid of the DnsGly. The PL intensity is higher for the MCM-41@Ch@DnsGly NPs than for the pristine dansylglycine, since the NP is covered by dansylglycine moieties, increasing its fluorescence.

The fluorescence behaviour of the MCM-41@Ch@DnsGly NPs as a function of excitation wavelength (λ_{ex}) is shown in Fig. 4b. $\lambda_{\text{em}} = 515$ nm, independent of λ_{ex} , but the PL intensity is

maximum when $\lambda_{\text{ex}} = 360$ nm. This implication of this characteristic in the forensic context is discussed in the next section, with regard to optimizing optical contrast between the developed fingerprint and substrate, and minimizing background fluorescence from the substrate (particularly in the cases of plastic and paper).

Development of latent fingerprints

Latent fingerprints present on different substrates (glass, plastic, stainless steel and unfired brass cartridge cases) were developed by using the MCM-41@Ch@DnsGly NPs and visualized under UV light (365 nm). Bright fluorescent images of the developed fingerprints could be clearly seen under illumination by visible (Fig. 5b) or UV (Fig. 5c–f) light.

Among the variables that can affect the quality of developed fingerprint images, the residue age and composition are of primary forensic significance, since most conventional methods involve physical or chemical interaction between the developing agent and one or more components of the fingerprint residue. Evaporation from the mark of water and the residual mixture of organic and inorganic compounds ultimately results in accumulation of the less volatile components into a waxy layer.^{57–59} With some variation according to the environment (notably temperature and humidity), the most significant compositional changes occur within the first few days. The outcome is that the fingerprint ridges become thinner and extent of fine detail diminishes; essentially the fidelity of the available image degrades. Thus, visualization of aged latent fingerprints based on adhesion/interaction of the developing agent with the sweat and sebaceous residues can become challenging for conventional materials.⁵⁹

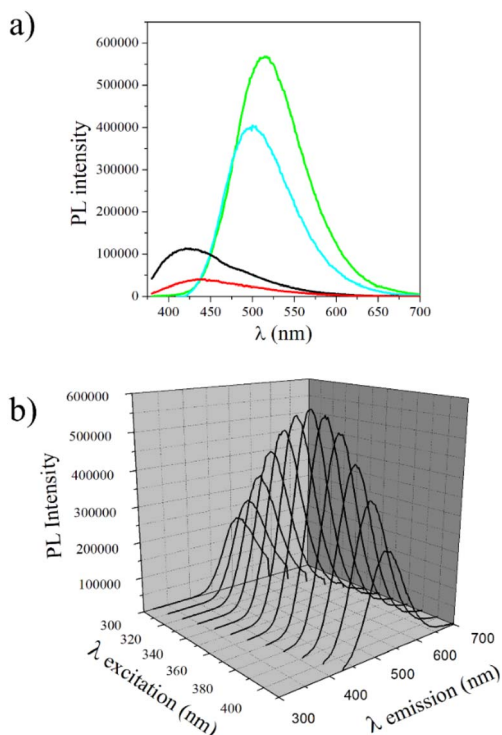


Fig. 4 Fluorescence spectra for (a) MCM-41 (—), MCM-41@Ch (—), DnsGly (—), and MCM-41@Ch@DnsGly (—) with $\lambda_{\text{ex}} = 360$ nm, and (b) MCM-41@Ch@DnsGly illuminated at different excitation wavelengths (λ_{ex}).

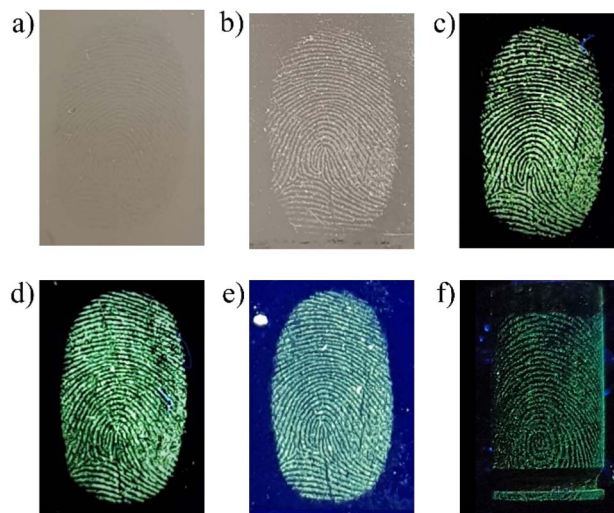


Fig. 5 Representative images of latent fingerprints on stainless steel illuminated by and viewed under visible light (a) before development and (b) after development with MCM-41@Ch@DnsGly NPs. Corresponding images generated by illumination with UV light ($\lambda_{\text{ex}} = 365$ nm) by MCM-41@Ch@DnsGly NP development on (c) stainless steel, (d) glass, (e) plastic and (f) unfired brass cartridge case substrates.

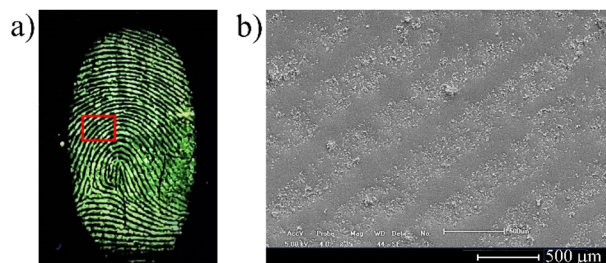


Fig. 6 Representative image of (a) 30 day old fingerprint on stainless steel developed by applying MCM-41@Ch@DnsGly NPs together with (b) SEM image showing the NPs (clusters) preferentially deposited on the fingerprint ridges.

Additionally, dansyl derivatives are known as fluorescent probes for determination of certain human proteins, free amino acids, and biologically generated halogenated compounds,^{60,61} making this class of fluorophores able to effectively interact with the fingerprint residue.⁴⁵ As shown in Fig. 6, delivery to the surface by the NPs of a high population of fluorophores, combined with their high PL intensity offers the potential to overcome this ageing effect. From SEM analysis it was possible to observe that the MCM-41@Ch@DnsGly NPs bind preferentially to latent fingerprint ridges, allowing the enhancement of latent fingerprints with high contrast images and clear visualization of fingerprint patterns, even on aged (30 days) fingerprinted surfaces, Fig. 6 (see also Fig. S2, ESI†).

Fingerprint detection and enhancement is commonly performed using excitation from a suitable forensic light source, with direct image capture onto a high sensitivity charge-coupled device camera. For luminescent marks, a suitable barrier filter is required to block the reflected excitation light and selectively transmit the developed fingerprint emission; use of filters spanning a wide spectral range permits optimization of image contrast.⁶² The developed fingerprints were illuminated with light in the wavelength range from 365 to 640 nm and observed *via* filters of longer wavelength than the excitation light (since emission is at longer wavelengths than absorption). Observations using all available illumination sources and viewing filters were analyzed to yield the optimum illumination/filter

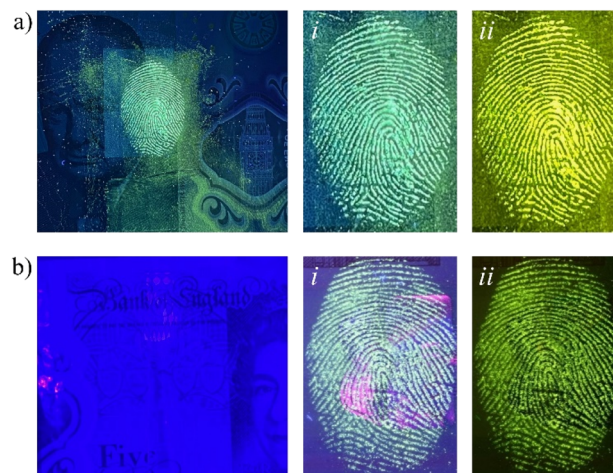


Fig. 8 Fingerprint developed using MCM-41@Ch@DnsGly NPs on a £5 banknote: (a) back security feature illuminated at 365 nm and viewed with no filter (i) and 510 nm filter (ii) (b) holographic foil illuminated at 365 nm and viewed with no filter (i) and a 510 nm filter (ii).

combination (see Fig. S3, ESI†). Representative data are shown in Fig. 7 for a fingerprint on glass visualized with MCM-41@Ch@DnsGly NPs, illuminated at 365 nm (see Fig. 5) and viewed using filters from 435 to 624 nm.

One of the main applications for multispectral imaging and monochromatic illumination is for improvement of developed fingerprints on surfaces presenting topographically, optically, and chemically complex backgrounds. The patterned and/or multicolored backgrounds used as security features on banknotes are a prime example. As an example, UK banknotes show fluorescent patterns, microprinting, transparent areas, holographic foil and raised sections, all of which contribute to the challenge of visualising latent fingerprints. The capability of MCM-41@Ch@DnsGly NPs to generate strong enhancement of latent fingerprints selectively contrasted against background interference in these areas is illustrated in Fig. 8. The only substantive limitation is associated with the holographic foil, from which reflectance results in some glare; this could be overcome by the correct application of viewing filters.

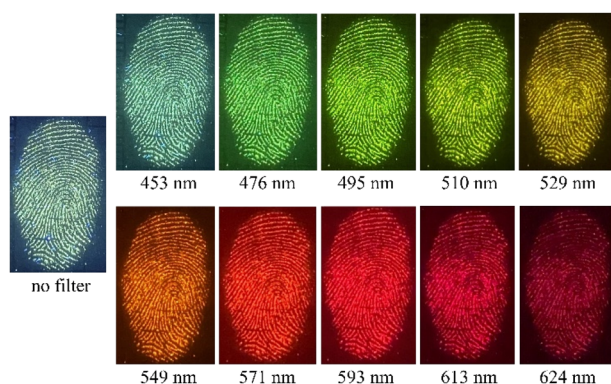


Fig. 7 Images for a fingerprint deposited on glass, enhanced with MCM-41@Ch@DnsGly NPs, illuminated at 365 nm and viewed with different filters (as indicated).

Image analysis

Quality assessment tools for developed fingerprint images are important to attest the effectiveness of the material and/or methodology proposed. These include grading schemes,⁶³ forensic protocols^{1,64} and forensic software for fingerprint recognition and analysis, and provide a link between research and practitioner environments. An individual can be identified through matching the stored fingerprints in a database with the image of its developed fingerprint. Usually, the whole pattern of the mark will first be compared to narrow down the search range and then some minutiae, if available, will be analyzed to complete the identification. This is a convenient process since powerful computer and information analysis techniques are present at most forensic laboratories.



The efficacy of the fluorescent NPs in the latent fingerprint enhancement was evaluated by the analysis of the images of all samples of developed fingerprints, including the different donors (1 male and 4 female), surfaces (stainless steel, glass, plastic, unfired brass cartridge cases and banknotes) and ages of the fingerprint residue (fresh, 1, 7, 15 and 30 days), by using the UK Home Office scale and a forensic software that enables the identification of the main details of the fingerprint, such as characteristic minutiae and pores. A total of 66 images were graded according to the UK Home Office five-point scale running from 0 (no development) to 4 (full development), depending upon the quantity of clear ridge detail taking into account the continuous ridge flow (see Table S1, ESI†).^{1,63,64} Although this scale is designed for research rather than legal application, it is broadly accepted that images of grades 3 and 4 would provide unequivocal identification.⁶³ In the present study, 94% of the samples satisfied this “whole image” based criterion.

Moving to the details of the friction ridge skin features, these can be classified into three levels: level 1 provides the pattern information (arches, loops, whorls) of the fingerprint; level 2 describes the minutiae, including core, bifurcation, delta, bridge, enclosure, termination, island, short ridge, and hook;

and level 3 refers to ridge shape, and the number and location of sweat pores.⁶⁵ With suitable magnification and image analysis using the forensic software, levels 1, 2 and 3 detail could be easily observed in the MCM-41@Ch@DnsGly NP enhanced latent fingerprints (see Fig. 9).

From the forensic software analysis in representative images, it was possible to identify between 14–38 minutiae, depending on the surface on which the fingerprint was present (see Fig. 9 and S4, ESI†). Flat surfaces, such as stainless steel plates (38 minutiae), glass (24 minutiae), plastic (30 minutiae) and banknotes (37 minutiae) allow the interpretation of the whole image by the software to find a great number of minutiae, whilst the cylindrical surface of the cartridge case makes image analysis more difficult, as commonly observed in forensic practice. This is particularly true for the minutiae present at the edges, since the software analyses a two dimensional image registered from a three dimension object and is thus vulnerable to distortion. Even so, at least 14 minutiae could be found in the analysis of the developed fingerprints on cartridge cases by the forensic software. We conclude that combination of visual inspection (Home Office grading system) and image treatment using forensic software is a powerful means of identifying ridge patterns, fingerprint class distinction and minutiae of the MCM-41@Ch@DnsGly NP developed fingerprints. These twin approaches address issues of quantity and quality (94% at grade 3 or 4; and >24 minutiae) that satisfy criteria for safe and robust forensic comparison examination with reference dactyloscopy images to provide unambiguous identification of an individual.

Conclusions

A fluorescent nanoparticle based on hierarchical MCM-41@Ch@DnsGly hybrid structure was synthesized, characterized and applied as a latent fingerprint developer. Due to the small size and functionalization of MCM-41 with chitosan and dansylglycine, the so produced nanoparticle presented fluorescence properties, and strong interaction with specific components (e.g., amino acids, fatty acids) of the fingerprint residue, which provided high adhesion of the nanoparticles, even for aged fingerprints. The fluorescence characteristics of the hybrid material were exploited for the development of latent fingerprints on different surfaces, including metal, plastic and glass. From a pseudo-operational perspective, this material has been successfully applied for visualization of latent fingerprints on polymer banknotes with complex background (holographic markers, color and textures).

Nanostructured MCM-41@chitosan@dansylglycine particles have been demonstrated to provide high quality images of latent fingerprints for substrates with spatially varying topography, composition and colour; the portfolio of holographic and other security features on polymer banknotes exemplifies the point. The fundamental capability, and the ability to realize it without laboratory facilities (*i.e.* at a crime scene), represents a substantive advance over the performance of other dansylglycine materials, such as the electrospun PCL/dansylglycine nanofibers described previously in ref. 45.

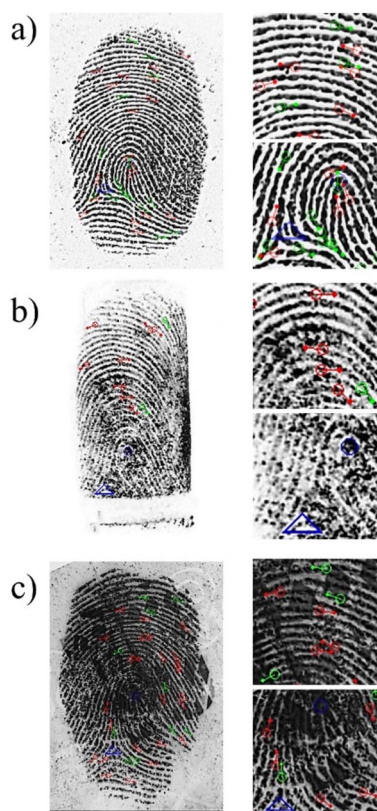


Fig. 9 Representative binarized (B&W) images of developed latent fingerprints on (a) stainless steel, (b) unfired brass cartridge case and (c) UK banknote. In each row, the left hand image shows the whole mark with level 1, 2 and 3 details identified: ridge ending (red), bifurcation (green), delta (blue triangle) and core (blue circle). Images in the right hand column show magnified sections of the mark, similarly annotated using the forensic software.



Developed image quality has been assessed by the UK Home Office grading scheme: 94% of the nanoparticle enhanced images were grade 3 or 4 (carrying the expectation of a successful identification). The smaller features (second and third level detail) whose unique spatial relationship is the basis of identification of an individual, were readily recognized using forensic software. The experimental evidence unequivocally shows that MCM-41@Ch@DnsGly NPs allow the acquisition of images of identification standard; the protocol generating such images is straightforward, rapid, reliable and consistent with the legal identification of an individual (including ethical compliance). Preliminary application in the forensic environment indicates that this concept offers substantive near term future promise for latent fingerprint development and identification in forensic investigations.

Experimental section

Materials

Tetraethyl orthosilicate (TEOS, 99%), *N*-cetyl-*N,N,N* trimethyl ammonium bromide (CTAB), (3-aminopropyl)triethoxysilane (APTES, 99%), dansylglycine (DnsGly), anhydrous acetonitrile (CH₃CN, 99.8%), absolute ethanol, anhydrous chloroform (CHCl₃, ≥ 99%), glacial acetic acid (HAc, 99.7%) and ammonium hydroxide (NH₄OH, 25–28 wt%) were purchased from Sigma-Aldrich (St. Louis, MO, USA). Chitosan (deacetylation degree 85%; Mw 100 000–300 000) was provided by Acros Organics. All reagents were used as received.

Synthesis of mesoporous silica nanoparticles MCM-41

MCM-41 samples were prepared by a CTAB-templated co-condensation method,²⁹ adapted from the procedure described by Basumatary *et al.*⁴⁹ First, deionized H₂O (500 mL) was heated at 50 °C, then NH₄OH (26.4 mL, 28.7 wt%) was added to adjust the pH to ~11, followed by the addition of CTAB (0.56 g). The solution was stirred for 15 min for complete homogenization. After that, TEOS (2.9 mL) was added dropwise under magnetic stirring and the mixture was left for 2 hours at 50 °C. The resulting sample was centrifuged at 8000 rpm for 5 min and washed twice with ultrapure H₂O and ethanol until neutral pH, and finally dried at 80 °C overnight. To remove the CTAB template, the resulting material was calcined under atmospheric conditions at 550 °C for 4 hours at a heating rate of 5 °C min⁻¹.

Functionalization of MCM-41 with chitosan

Modification of the MCM-41 surface with chitosan was performed according to the procedure reported by Gan *et al.*⁵² A 1% chitosan solution was prepared by dissolving chitosan (0.5 g) in 50 mL of aqueous 5% HAc solution, under vigorous magnetic stirring for 24 hours. Then, MCM-41 (0.1 g) was added to 10 mL of ethanol and kept in an ultrasonic bath for 1 hour. After this time, the solution was left under vigorous stirring and the pH was adjusted to 3.5–4.5 with HAc, then 0.1 mL of APTES was added to the mixture and the stirring was maintained for 3 hours. The previously prepared 1% chitosan solution (20 mL) was added to

the reaction mixture and left for 24 hours under stirring at room temperature (25 °C). In the next step the solution was centrifuged at 8000 rpm for 5 minutes, washed twice with deionized water and then dried under reduced pressure.

Functionalization of MCM-41@Ch with dansylglycine

A solution of DnsGly (5.0 mg) in dry CH₃CN (5.0 mL) was added to MCM-41@Ch (100 mg). The mixture was maintained under magnetic stirring at 100 rpm for 24 hours, then centrifuged for 3 minutes at 5000 rpm. The reaction product was washed with CHCl₃ until the supernatant did not exhibit fluorescence, then dried at room temperature for 24 h.

Characterization

FTIR spectra were recorded using a Shimadzu IR Prestige-21 spectrophotometer. The morphology of the samples was assessed by scanning electron microscopy (SEM) (Superscan SSX-550; Shimadzu). High-resolution X-ray diffraction (XRD) patterns of powdered samples were recorded on a Shimadzu XRD-6000 X-ray diffractometer using Cu K α radiation ($\lambda = 1.79$ Å). Small angle X-ray scattering (SAXS) results were generated using the Diamond Light Source DL-SAXS lab SAXS instrument, using the Genix3D Molybdenum Micro-Source producing 17.4 keV photons. Signals were detected using an Eiger R 1M (SAXS) (75 micron) detector. Powder samples were sealed in Kapton disks with Scotch Magic Tape and sealed in the sample holder with 15 mm \times 6 mm \times 0.75 mm spacing. Samples were held 808.15 mm from the beam and distance was confirmed using silver behenate (AgBeh) as the calibrant. Measurements were made with a 1.4 mm slit opening and were measured for 2.5 hours. Data was processed using DAWN according to the procedure described by Filik *et al.*⁶⁶ TEM images were obtained using a transmission electron microscope, with Tecnai Spirit T12 analysis. Nanoparticle average diameters were calculated using ImageJ (NIH, Bethesda, MD) after measuring 100 nanoparticles from each sample. For solid-state fluorescence analysis the powder samples were placed into the solid sample holder accessory of the Fluorolog Horiba Jobin Yvon spectrofluorometer and the fluorescence emission spectra were recorded by front-face (30°) detection.

Fingerprint collection and development process

Prior to fingerprint collection, donors (4 female and 1 male) washed their hands with soap and dried them with paper towel. Then, they rubbed their fingers over the oily parts of the body like the retroauricular, forehead and nose regions to ensure deposition of a rich and even sebaceous fingerprint. Then, the donors deposited their fingerprints on the substrates (glass slides, stainless steel plates, transparency plastic sheets, unfired cartridge cases and UK bank notes) by contact with the surface for 1–2 seconds with minimal pressure.⁶⁴ Written consent from all participants was obtained prior to the research and it was approved by Brazilian Ethics Committee (Plataforma Brasil, CAAE 42419221.2.0000.5013). The collected fingerprints were stored in a covered box under ambient conditions for further use.



For the development process, MCM-41@ChS@DnsGly NPs were gently spread on the fingermark, then the surface was tilted and carefully tapped to remove unattached particles. This procedure was carried out over a watch glass to collect non-adherent particles. The as-developed fingerprints were photographed with a Nikon D5500 professional camera under visible and UV light sources or a modified Nikon D6 camera with 20.8 million effective pixels and the DCS5 imaging system (Foster & Freeman, Evesham, UK). Fingermarks were illuminated and viewed using a Crime-lite 8X4 MK2 (Foster & Freeman), consisting of 32 high intensity LEDs with illumination at 7 different wavelengths (365–640 nm) and 12 slot-in fluorescence viewing filters ranging from 435 to 624 nm. The images obtained from the developed fingerprints were analyzed by applying forensic protocols, including the UK Home Office grading scale⁶⁴ (at whole image level) and the Griaule® Forensic Fingerprint v.1.1 software, through scientific collaboration with the National Criminalistics Institute of the Federal Police of Brazil (to identify individual minutiae).

Data availability

Data supporting this article have been included as part of the ESI.†

Author contributions

Conceptualization by A. S. R., A. R. H., and T. G. N. Methodology by A. R. H., L. F. A. M. O., M. S. A., N. R., P. T. W., T. Z., and A. M. L. A., Validation by L. F. A. M. O., M. S. A., C. V. C., J. C. S. M., and A. M. L. A. Formal analysis by A. R. H., M. S. A., C. V. C., J. C. S. M., A. M. L. A., and A. S. R. Investigation and data curation by L. F. A. M. O., L. V. A. T. S., A. F. S., M. S. A., C. V. C., J. C. S. M., and P. T. W. Resources by T. G. N., E. J. S. F., and A. S. R., writing – original draft by L. F. A. M. O. Visualization by A. R. H., M. S. A., and A. S. R. Supervision by A. R. H., L. F. A. M. O., T. G. N., E. J. S. F., and A. M. L. A. Writing – review & editing by A. R. H., A. M. L. A., and A. S. R. Project administration and funding acquisition by A. S. R.

Conflicts of interest

There are no conflicts to declare.

Acknowledgements

The authors wish to thank the granting authorities FAPEAL (process 60030.0000001635/2022), CNPq and CAPES for financial support. The authors also are grateful to EPSRC as the funder of the Diamond Leeds SAXS Facility (grant no. EP/R042683/1), and National Institute of Criminalistics of the Brazilian Federal Police for technical support.

References

- 1 C. Champod, C. Lennard, P. Margot and M. Stoilovic, *Fingerprints and Other Ridges Skin Impressions*, CRC Press, Boca Raton, FL, 2nd edn, 2016.
- 2 C. Lennard, *Aust. J. Forensic Sci.*, 2020, **52**, 125.
- 3 M. Wang, M. Li, A. Yu, Y. Zhu, M. Yang and C. Mao, *Adv. Funct. Mater.*, 2017, **27**, 1606243.
- 4 O. P. Jasuja, P. Kumar and G. Singh, *Sci. Justice*, 2015, **55**, 335.
- 5 G. S. Sodhi and J. Kaur, *Forensic Sci. Int.*, 2001, **120**, 172.
- 6 UK Home Office Centre for Applied Science and Technology CAST, *Fingerprint Visualisation Manual*, The Stationary Office, 1st edn, 2014.
- 7 K. C. O'Neill, P. Hinners and Y. J. Lee, *J. Forensic Sci.*, 2018, **63**, 1854.
- 8 G. Kolhatkar, C. Parisien, A. Ruediger and C. Muehlethaler, *Front. Chem.*, 2019, **7**, 440.
- 9 J. Xu, Z. Zhang, X. Zheng and J. W. Bond, *J. Forensic Sci.*, 2017, **62**, 776.
- 10 C. Yuan, M. Li, M. Wang, H. Cao and T. Lin, *Electrochim. Acta*, 2021, **390**, 138798.
- 11 C. V. Costa, A. M. L. Assis, J. D. Freitas, J. Tonholo and A. S. Ribeiro, *Nano Sel.*, 2020, **1**, 405.
- 12 R. M. Sapstead, N. Corden and A. R. Hillman, *Electrochim. Acta*, 2015, **162**, 119.
- 13 A. L. Beresford and A. R. Hillman, *Anal. Chem.*, 2010, **82**, 483.
- 14 R. M. Brown and A. R. Hillman, *Phys. Chem. Chem. Phys.*, 2012, **14**, 8653.
- 15 R. M. Sapstead (nee Brown), K. S. Ryder, C. Fullarton, M. Skoda, R. M. Dalglish, E. B. Watkins, C. Beebe, R. Barker, A. Glidle and A. R. Hillman, *Faraday Discuss.*, 2013, **164**, 391.
- 16 C. V. Costa, L. I. M. Gama, N. O. Damasceno, A. M. L. Assis, W. M. G. Soares, R. C. Silva, J. Tonholo and A. S. Ribeiro, *Synth. Met.*, 2020, **262**, 116347.
- 17 M. S. Alves, J. C. S. Melo, C. V. Costa, M. Ula, J. D. de Freitas, J. Tonholo, A. R. Hillman, A. M. L. de Assis and A. S. Ribeiro, *Electrochim. Acta*, 2024, **484**, 143925.
- 18 V. Prasad, S. Lukose, P. Agarwal and L. Prasad, *J. Forensic Sci.*, 2020, **65**, 26.
- 19 E. Prabakaran and K. Pillay, *J. Mater. Res. Technol.*, 2021, **12**, 1856.
- 20 J. Lian, F. Meng, W. Wang and Z. Zhang, *Front. Chem.*, 2020, **8**, 594864.
- 21 A. M. L. Assis, C. V. Costa, M. S. Alves, J. C. S. Melo, V. R. Oliveira, J. Tonholo, A. R. Hillman and A. S. Ribeiro, *WIREs Forensic Sci.*, 2023, **5**, e1475.
- 22 B. M. F. Costa, D. V. Freitas, F. L. N. Sousa, K. D. Silva, J. M. M. Dias, A. M. L. Assis, A. C. Jesus, A. S. Ribeiro and M. Navarro, *Dyes Pigm.*, 2020, **180**, 108483.
- 23 R. Bahadur, M. K. Kumawat, M. Thakur and R. Srivastava, *J. Lumin.*, 2019, **208**, 428.
- 24 R. Rajan, Y. Zakaria, S. Shamsuddin and N. F. N. Hassan, *Egypt. J. Forensic Sci.*, 2019, **9**, 50.
- 25 W. Huang, X. Li, H. Wang, X. Xu, H. Liu and G. Wang, *Anal. Lett.*, 2015, **48**, 1524.



- 26 S. Zhang, R. Liu, Q. Cui, Y. Yang, Q. Cao, W. Xu and L. Li, *ACS Appl. Mater. Interfaces*, 2017, **9**, 44134.
- 27 Y. J. Kim, H. S. Jung, J. Lim, S. J. Ryu and J. K. Lee, *Langmuir*, 2016, **32**, 8077.
- 28 H. Zhang, J. You, C. Nie, J. Wang, X. Dong, R. Guan, D. Cao and Q. Chen, *J. Lumin.*, 2019, **215**, 116582.
- 29 L. F. A. M. Oliveira, L. V. A. T. da Silva, T. G. do Nascimento, L. M. de Almeida, R. J. N. Calumby, A. M. Nunes, L. M. T. M. Oliveira and E. J. S. Fonseca, *Drug Dev. Ind. Pharm.*, 2020, **46**, 1199.
- 30 A. Mehmood, H. Ghafar, U. F. Gohar and B. Ahmad, Mesoporous silica nanoparticles: a review, *J. Dev. Drugs*, 2017, **6**, 1000174.
- 31 R. K. Kankala, Y.-H. Han, J. Na, C.-H. Lee, Z. Sun, S.-B. Wang, T. Kimura, Y. S. Ok, Y. Yamauchi, A.-Z. Chen and K. C.-W. Wu, *Adv. Mater.*, 2020, 1907035.
- 32 Q. Li, W. Wang, G. Hu, X. Cui, D. Sun, Z. Jin and K. Zhao, *Molecules*, 2021, **26**, 2490.
- 33 Y. Hu, L. Le, H. Chen, M. Zhuo, X. Yang, D. Zhao, S. Zhung and X. Xiao, *Int. J. Nanomed.*, 2017, **12**, 8411.
- 34 Z. Shakeran, M. Keyhanfar, J. Varshosag and D. S. Sutherland, *Mater. Sci. Eng., C*, 2021, **118**, 111526.
- 35 J.-T. Lin, Z.-K. Liu, Q.-L. Zhu, X.-H. Rong, C.-L. Liang, J. Wang, D. Ma, J. Sun and G. H. Wang, *Colloids Surf., B*, 2017, **155**, 41.
- 36 L. Alison, P. A. Rühls, E. Tervoort, A. Teleki, M. Zanini, L. Isa and A. R. Studart, *Langmuir*, 2016, **32**, 13446.
- 37 E. M. A. Hejjaji, A. M. Smith and G. A. Morris, *Food Hydrocolloids*, 2017, **71**, 290.
- 38 N. Vučković, N. Glodović, Z. Radovanović, D. Janačković and N. Milašinović, *J. Forensic Sci.*, 2021, **66**, 149.
- 39 T. G. do Nascimento, N. M. do Nascimento, A. S. Ribeiro, C. P. de Almeida, J. I. Z. dos Santos, I. D. Basilio-Júnior, F. G. C. Calheiros-Silva, G. M. Lira, P. B. Escodro, I. C. C. M. Porto, V. A. da Silva, C. B. Dornelas, J. S. Sousa and J. D. de Freitas, *J. Therm. Anal. Calorim.*, 2021, **147**, 7837.
- 40 A. P. P. Praxedes, G. D. Weber, S. T. Souza, A. S. Ribeiro, E. J. S. Fonseca and I. N. de Oliveira, *Appl. Surf. Sci.*, 2016, **370**, 25.
- 41 R. C. Silva, M. V. Sarmiento, F. A. R. Nogueira, J. Tonholo, R. J. Mortimer, R. Faez and A. S. Ribeiro, *RSC Adv.*, 2014, **4**, 14948.
- 42 R. C. Silva, M. V. Sarmiento, R. Faez, R. J. Mortimer and A. S. Ribeiro, *J. Braz. Chem. Soc.*, 2016, **27**, 1847.
- 43 A. J. C. Silva, J. G. Silva Jr, S. Alves Jr, J. Tonholo and A. S. Ribeiro, *J. Braz. Chem. Soc.*, 2011, **22**, 1808.
- 44 A. P. P. Praxedes, A. J. C. da Silva, R. C. da Silva, R. P. A. Lima, J. Tonholo, A. S. Ribeiro and I. N. de Oliveira, *J. Colloid Interface Sci.*, 2012, **376**, 255.
- 45 E. G. Mazzini Júnior, J. D. A. Cantalice, A. M. L. de Assis, J. D. de Freitas, L. M. M. Costa and A. S. Ribeiro, *J. Appl. Polym. Sci.*, 2020, **137**, 49804.
- 46 J. B. Friesen, *J. Chem. Educ.*, 2015, **92**, 497.
- 47 A. J. Parola, J. C. Lima, F. Pina, J. Pina, J. S. de Melo, C. Soriano, E. Garcia-España, R. Aucejo and J. Alarcón, *Inorg. Chim. Acta*, 2007, **360**, 1200.
- 48 D. S. Bhagat, P. B. Chavan, W. B. Gurnule, S. K. Shejul and I. V. Suryawanshi, *Mater. Today: Proc.*, 2020, **29**, 1223.
- 49 A. K. Basumatary, R. V. Kumar, A. K. Ghoshal and G. Pugazhethi, *J. Membr. Sci.*, 2015, **475**, 521.
- 50 N. Moradpour, S. Sedaghat, P. A. Azar and K. Behzad, *Appl. Organomet. Chem.*, 2021, **35**, e6277.
- 51 S. Elderderi, C. Leman-Loubière, L. Wils, S. Henry, D. Bertrand, H. J. Byrne, I. Chourpa, C. Enguehard-Gueffier, E. Munnier, A. A. Elbashir, L. Boudesocque-Delaye and F. Bonnier, *J. Mol. Liq.*, 2020, **311**, 113361.
- 52 Q. Gan, J. Zhu, Y. Yuan, H. Liu, J. Qian, Y. Li and C. Liu, *J. Mater. Chem. B*, 2015, **3**, 2056.
- 53 M. K. Amin and J. S. Boateng, *J. Pharm. Sci.*, 2020, **109**, 2271.
- 54 L. Guo, H. Sato, T. Hashimoto and Y. Ozaki, *Macromolecules*, 2010, **43**, 3897.
- 55 M. A. Sibeko, M. L. Saladino, A. S. Luyt and E. Caponetti, *J. Mater. Sci.*, 2016, **51**, 3957.
- 56 J. Tovar-Rodriguez, E. Fratini, P. Baglioni, C. Ferrari, J. A. de los Reyes-Heredia, Y. Ramírez-Hernández and I. R. Galindo-Esquivel, *Nanomaterials*, 2023, **13**, 997.
- 57 A. Girod, R. Ramotowski and C. Weyermann, *Forensic Sci. Int.*, 2012, **223**, 10.
- 58 A. Girod and C. Weyermann, *Forensic Sci. Int.*, 2014, **238**, 68.
- 59 S. Cadd, M. Islam, P. Manson and S. Bleay, *Sci. Justice*, 2015, **55**, 219.
- 60 S. Wang, B. G. Vigliarolo, M. A. Chowdhury, J. N. K. Nyarko, D. D. Mousseau and C. P. Phenix, *Bioorg. Chem.*, 2019, **92**, 103194.
- 61 L. C. Bertozzo, M. L. Zeraik and V. F. Ximenes, *Anal. Biochem.*, 2017, **532**, 29.
- 62 D. L. Exline, C. Wallace, C. Roux, C. Lennard, M. P. Nelson and P. J. Treado, *J. Forensic Sci.*, 2003, **48**, 1047–1053.
- 63 H. I. Bandey, *Fingerprint Development and Imaging Newsletter: the Powders Process, Police Scientific Development Branch, Home Office, Sandridge, UK*, 2004.
- 64 V. G. Sears, S. M. Bleay, H. L. Bandey and V. J. Bowman, *Sci. Justice*, 2012, **52**, 145.
- 65 C. Wang, J. Zhou, L. Lulu and Q. Song, *Part. Part. Syst. Charact.*, 2018, **35**, 1700387.
- 66 J. Filik, A. W. Ashton, P. C. Y. Chang, P. A. Chater, S. J. Day, M. Drakopoulos, M. W. Gerring, M. L. Hart, O. V. Magdysyuk, S. Michalik, A. Smith, C. C. Tang, N. J. Terrill, M. T. Wharmby and H. Wilhelm, *J. Appl. Crystallogr.*, 2017, **50**, 959.

